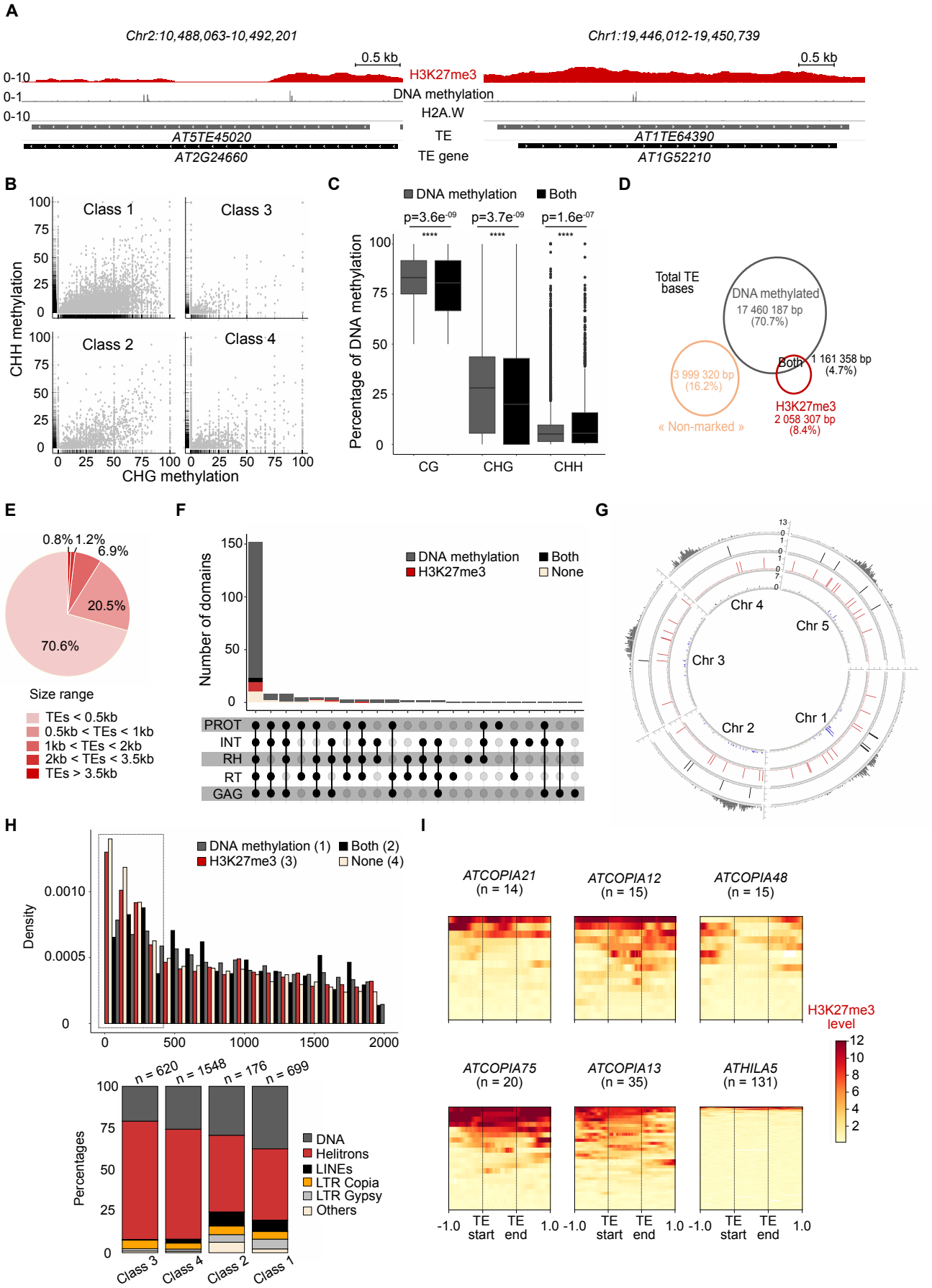

Fig S1. Many TE are marked by H3K27me3 in wild type Arabidopsis (Col-0)
(A) Representative genome browser view of H3K27me3 (red), DNA methylation (grey) and constitutive heterochromatin histone variant H2A.W (grey) levels in wild-type (WT) for two TEs marked by H3K27me3 in WT. Grey and black bars represent TEs and TE-genes annotations, respectively. **(B)** Plots showing CHG and CHH levels per TE in each class. **(C)** Box plot showing the CG, CHG and CHH methylation levels for each TE in class 1 and 2. Statistical analysis was performed using Wilcoxon-Mann-Whitney U-test. **(D)** Venn diagram showing the proportion of TE length for each class previously identified. **(E)** Pie chart showing proportion of size range among TE marked by H3K27me3 (Class 3). **(F)** UpSet plot depicting the combination of functional domain for the long TEs of each class. GAG, Group-specific antigens or Capsid protein; PR, protease; INT, integrase; RT, reverse-transcriptase; RH, ribonuclease H. **(G)** Circos plot showing chromosomal distribution of TEs>3.5kb for each class from class 1 to class 4 (outside to inside, respectively) using 100kb bin size. **(H) Top panel**: Bar plot showing the distribution of closest distance from downstream gene (within a 2kb range where each bin corresponds to 50bp) for each class of TE. **Bottom panel**: Stacked bar plot showing distribution of TE superfamilies for TEs within 400bp upstream of genes. **(I)** Heatmaps based on H3K27me3 levels along each TE copy within one given TE family.

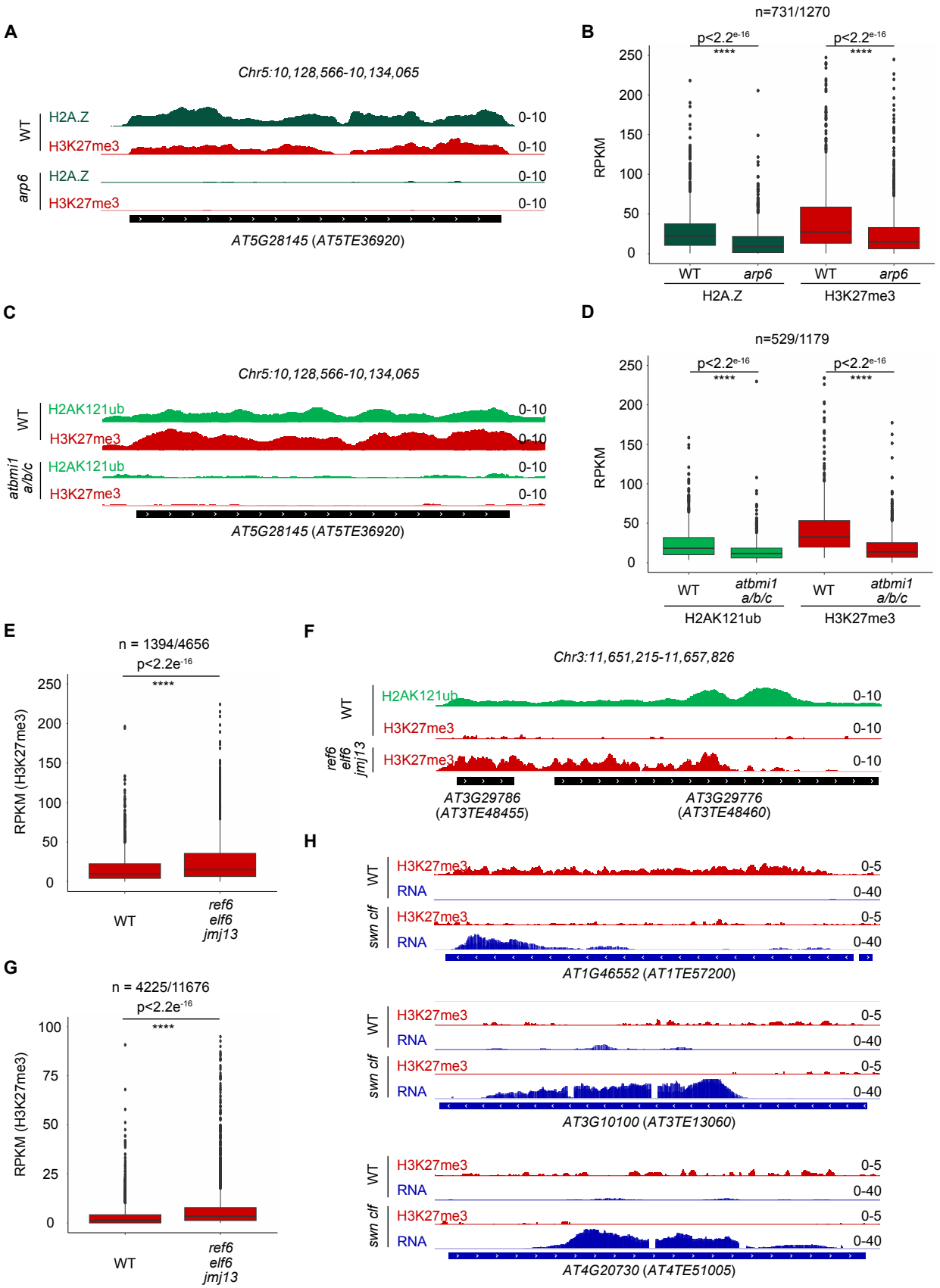

Fig S2. H3K27me3 at TEs can be associated with H2AUb and H2A.Z, active demethylation and transcriptional repression
(A) Representative genome browser view of TE in **Fig.2D** with CHIP-seq data in WT and in *arp6* mutant showing H2A.Z (dark green) and H3K27me3 (red) marks. **(B)** Boxplot showing H2A.Z (dark green) and H3K27me3 (red) levels for TEs that lose the marks in *arp6* mutant compared to WT. (**C)** Representative genome browser view of TE in **Fig.2E** with CHIP-seq data in WT and in *atbmi1a/b/c* triple mutant showing H2AK121ub (light green) and H3K27me3 (red). **(D)** Box plot showing H2AK121ub (light green) and H3K27me3 (red) levels for TEs that lose the marks in *atbmi1a/b/c* mutant compared to WT**. (E)** Boxplot showing H3K27me3 (red) levels for TEs marked by H3K27me3 in WT (class 3) that reach higher level of H3K27me3 in *ref6 elf6 jmj13***. (F)** Representative genome browser view of TE in **Fig.2F right panel** with CHIP-seq data in WT and in *ref6 elf6 jmj13* triple mutant showing H2AK121ub (light green) and H3K27me3 (red). **(G)** Boxplot showing H3K27me3 (red) levels for 'non-marked' TEs in WT (class 4) that gain H3K27me3 in *ref6 elf6 jmj13*. **(H)** Representative browser view of 3 TEs showing H3K27me3 (red) and RNA (blue) in WT and *swn clf* double mutant. Statistical analysis was performed using Wilcoxon-Mann-Whitney U-test.

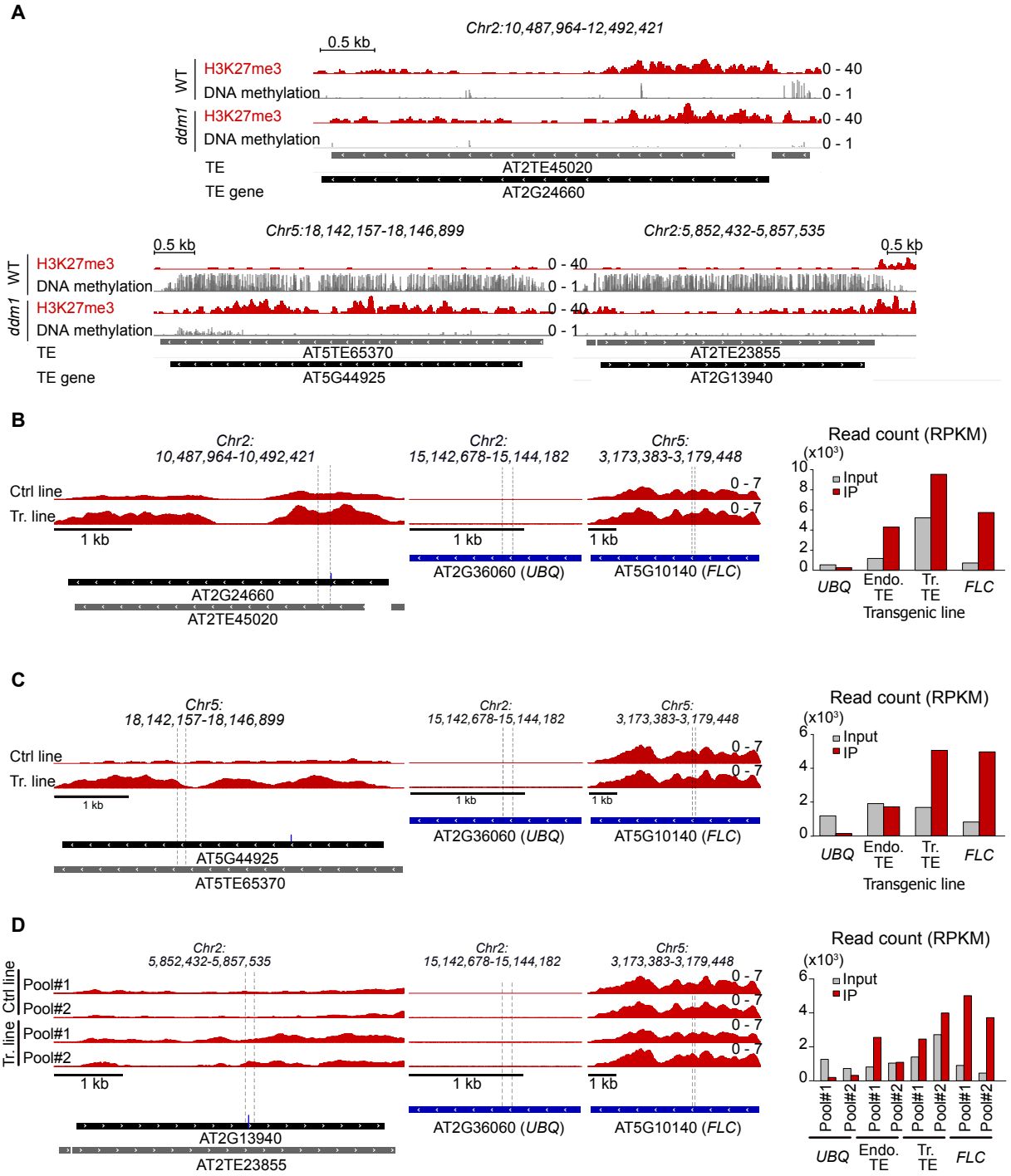

Fig S3. H3K27me3 can be recruited *de novo* and instructively at some transposable elements
(A) Presentation of the three individual TE sequences that were cloned into a binary vector. **(B-D)** Analyses of H37K27me3 on pools transformed with either *COPIA12B*, *COPIA21* and *COPIA13* as in Fig.3. The differences in profiles compared to Fig.3 and Fig.S2 is due to the use of another anti-H3K27me3 antibody in this experiment (Diagenode). **(B) Left panel.** Representative genome browser view of H3K27me3 average profile (IP-INPUT) at *COPIA12B* sequence (top panel) in a third independent pool of plants either transformed with unrelated transgene (Ctrl) or with the TE of interest. The H3K27me3 signal in the "Ctrl" tracks reflects the H3K27me3 status at the endogene TE. H3K27me3 signal in the "Tr" tracks reflects the H3K27me3 status at the endogene + transgene: higher signal compared to control line indicates recruitment of H3K27me3 on transgenic TEs in addition to the endogene. **Middle panel**: *UBQ* and *FLC* are the negative and positive controls respectively . **Right panel:** Recruitment on the transgene is determined by quantification of endogenous and transgenic *COPIA12B* sequences immunoprecipitated with H3K27me3 at the region where a SNP was introduced . ChIP-seq reads overlapping with the SNP at *COPIA12B* locus were extracted, counted and normalized by total read number. Recruitment on the transgene is validated by enrichment observed in IP as compared to an Input fraction. At control regions (*UBQ* and *FLC*), reads were extracted at positions *Chr5:3,178,750* (1st intron) and *Chr2:15,143,214* respectively). Copy number variation between transgenic pools can be visualized by the input DNA fraction (grey bar). In the non-transgenic lines, variation of input reflects difference in sequencing coverage at the SNP. **(C)** Left, middle and right panels are as in (B) for *COPIA21* sequence. **(D)** Left, middle and right panels as in (B) for COPIA13 sequence (2 independent transgenic pools are shown as well as two control pools).

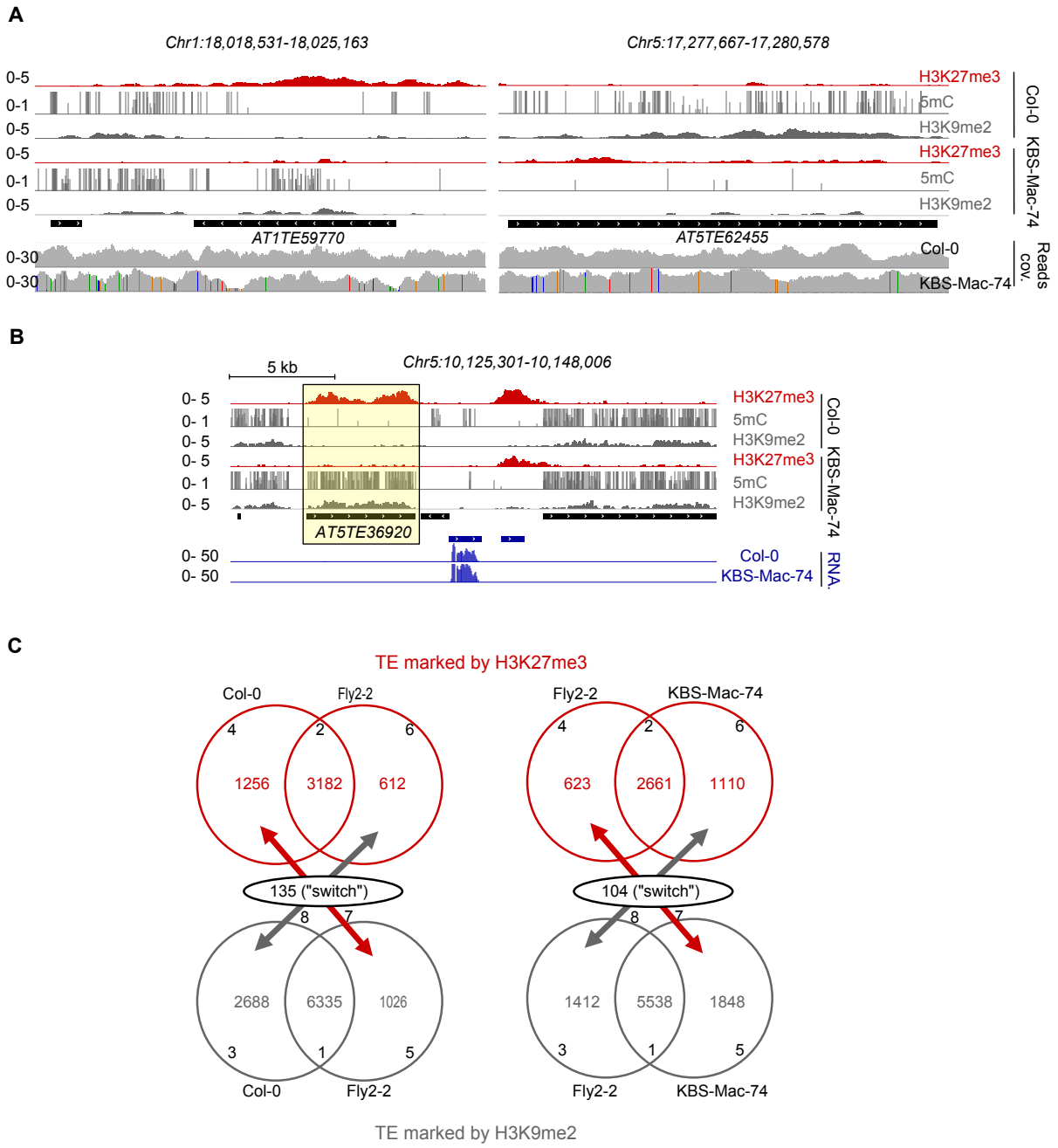

Fig S4. Switch between silencing epigenetic marks at TEs visualized by inter-accessions comparisons
H3K27me3 marks are in red, and DNA methylation (5mC) / H3K9me2 marks are in grey; TE annotations are shown as black bars. **(A)** Representative genome browser view of epigenetic switch at two orthologous TEs between Col-0 and KBS-Mac-74 (coverage and SNPs are shown). **(B)** Representative genome browser view of epigenetic switch at an orthologuous TE (*AT5TE36920)* with nearby regions shown, in Col-0 and KBS-Mac-74 accessions (Blue bars : Transcripts level). **(C)** Venn diagram of TEs marked by H3K27me3 (red circles), or by H3K9me2 (grey circles), in two different accessions, Col-0/Fly-2 (left panel) and Fly-2/KBS-Mac-74 (right panel). Intersection between both Venn diagrams show TEs that switch from H3K27me3 in one accession to H3K9me2 in the other.

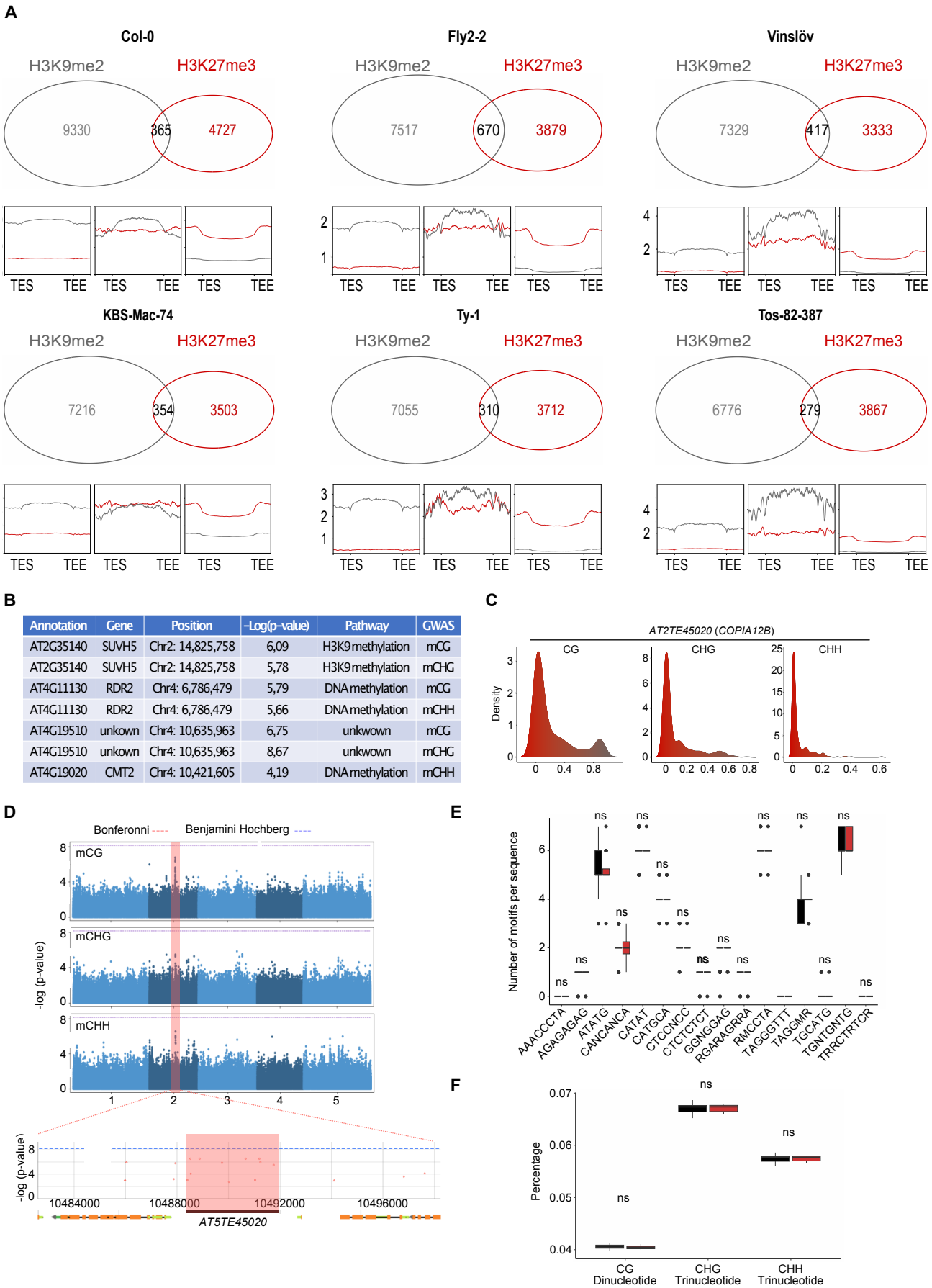

Annotation	Gene	Position	-Log(p-value)	Pathway	GWAS
AT2G35140	SUVH5	Chr2: 14,825,758	6,09	H3K9 methylation	mCG
AT2G35140	SUVH5	Chr2: 14,825,758	5,78	H3K9 methylation	mCHG
AT4G11130	RDR2	Chr4: 6,786,479	5,79	DNA methylation	mCG
AT4G11130	RDR2	Chr4: 6,786,479	5,66	DNA methylation	mCHH
AT4G19510	unkown	Chr4: 10,635,963	6,75	unkwown	mCG
AT4G19510	unkown	Chr4: 10,635,963	8,67	unkwown	mCHG
AT4G19020	CMT2	Chr4: 10,421,605	4,19	DNA methylation	mCHH

Fig S5. Genetic determinants of epigenetic switch
(A) Venn diagrams showing in 6 different accessions (Col-0 (6909), Fly2-2(6024), Vinslöv(9057), KBS-Mac-74(1741), Ty-1(5784), Tos-82-387(1254)), the number of TEs marked by either H3K9me2 (as a proxy for DNA methylation - left), or by H3K27me3 (right) or by both (middle), using data from *Kornienko et al., 2023*. TE with no peak detected for none of the marks are not shown. For each subset, associated average levels of H3K9me2 (grey) and H3K27me3 (red) are shown below in the metaplots. **(B)** Table showing *trans*-peaks found in GWAS of *AT5TE39620*. **(C)** Plot showing DNA methylation value for *COPIA12B* (*AT2TE45020*) and the density across accessions in the 3 contexts, CG, CHG and CHH. **(D)** Manhattan plots showing univariate GWAS mCG (**upper panel**), mCHG (**middle panel**) and mCHH (**lower panel**) for 2 TEs, **left panel**: *AT2TE45020* and **right panel**: *AT5TE36920*. Horizontal lines show genome wide significance (p = 0.05 after Bonferroni correction or after Benjamini Hochberg). Yellow boxes indicate peaks in *trans*-factors related to DNA methylation and pink boxes indicate *cis*-region of the TE. **(E)** Number of known PRE-like motifs previously shown to recruit PRC2/PRC1 at genes (*Berger et al., 2012; Qüesta et al., 2016; Yuan et al., 2016; Xiao et al., 2017; Zhou et al., 2018*) in *COPIA12D* sequences either H3K27me3-marked (red) or DNA methylated (black) across accessions.**(F)** Percentage of CG, CHG and CHH di/tri-nucleotides in *COPIA12D* sequences either H3K27me3-marked (red) or DNA methylated (black) across accessions. Statistical analysis was performed using Wilcoxon U-test; ns = not significant.